Editors' Suggestion

Unconventional superconductivity in the single-atom-layer alloy Si(111)-$\sqrt{3} \times \sqrt{3}$-(Tl, Pb)

T. Nakamura,[1] H. Kim,[2,*] S. Ichinokura,[1,†] A. Takayama,[1] A. V. Zotov,[3] A. A. Saranin,[3] Y. Hasegawa,[2] and S. Hasegawa[1]

[1]*Department of Physics, University of Tokyo, Hongo, Tokyo 113-0033, Japan*

[2]*The Institute for Solid State Physics, University of Tokyo, Kashiwa, Chiba 277-8581, Japan*

[3]*Institute of Automation and Control Processes, FEB RAS, 690041 Vladivostok, Russia and School of Natural Sciences, Far Eastern Federal University, 690000 Vladivostok, Russia*

(Received 1 June 2017; revised manuscript received 12 September 2018; published 16 October 2018)

We present results of low-temperature scanning tunneling microscopy/spectroscopy measurements on the one-atom-layer superconductor, Si(111)-$\sqrt{3} \times \sqrt{3}$-(Tl, Pb) which has a spin-split band structure due to the Rashba-Bychkov effect. It was revealed that it has a multiple superconducting gap Δ with significant anisotropy and sizable magnitude of $2\Delta/k_BT_C \sim 8.6$ (k_B is the Boltzmann constant and T_C is the critical superconducting temperature). Under the magnetic field, a dip structure was observed even at the core of the vortex. The dip structure was like a "pseudogap" because it remained up to 2 T, well above the upper critical magnetic field determined in the transport measurements ($\sim$0.7 T). This unconventional behavior suggests the possibility of spin-triplet Cooper pairs related to parity-broken superconductors.

DOI: 10.1103/PhysRevB.98.134505

The two-dimensional (2D) superconductors, which are thinner than the coherence length, have been studied for the last several decades. The first experimental stage of 2D superconductivity concerned ultrathin films with thickness of several nanometers [1]. Recently, it has moved to "atomic-layer superconductors," including metal-induced surface reconstructions on semiconductors and bilayer graphene [2–8]. In such 2D superconductors, unusual phenomena have been reported such as a large in-plane critical magnetic field beyond the Pauli limit [9,10] and higher critical temperature compared to bulk counterparts [11,12]. Therefore, the 2D superconductor is becoming a more and more fascinating research field today.

One of the most important features in 2D superconductors grown on crystal surfaces is broken space-inversion symmetry (SIS) in a direction perpendicular to the surface. Theory for superconductivity under broken SIS and strong spin-orbit coupling (Rashba-Bychkov effect) predicts mixing of spin-singlet and -triplet Cooper pairs (parity-broken superconductors) [13]. In fact, bulk superconductors without centrosymmetry in crystal structures show anomalously large upper critical fields which cannot be explained in the framework of conventional superconductivity [14,15]. Since the atomic-layer superconductors also have broken SIS, mixing of Cooper pairs could naturally occur in them. For example, an atomic layer of Pb on a Si substrate has been suggested to have a spin-triplet component of Cooper pairs even though most of its properties are dominated by disorder [16].

In this paper, we show that the one-atom-layer alloy of Tl and Pb grown on a Si substrate, Si(111)-$\sqrt{3} \times \sqrt{3}$-(Tl, Pb), where large spin splitting occurs at the Fermi level due to the Rashba-Bychkov effect [6,17], has an unconventional superconducting nature revealed by scanning tunneling microscopy/spectroscopy (STM/STS) observations. The shape of the experimental superconducting gap was reproduced by numerical calculations based on an anisotropic nodeless gap function. We also observed anomalous vortices having a pseudogap structure at the core under the magnetic field. The pseudogap remained up to 2 T, well above the critical magnetic field determined in the transport measurements [6]. These unusual results suggest the possibility of spin-triplet Cooper pairs related to the parity-broken superconductivity in the Si(111)-$\sqrt{3} \times \sqrt{3}$-(Tl, Pb) system.

All procedures from sample preparation to STM/STS measurement were performed in the same ultrahigh-vacuum (UHV) system, which was equipped with molecular beam epitaxy capability and *in situ* reflection high-energy electron diffraction (RHEED) and ultralow temperature STM system (Unisoku, USM-1300S with a Nanonis controller). It had a ^{3}He-cryostat and a superconducting magnet; the magnetic field up to 7 T was applied in the direction vertical to the sample surface. The temperature of the STM head reached below 0.5 K. The STM and STS measurements were performed in UHV with the PtIr tip. The clean Si(111)-7 $\times$ 7 substrate was prepared by flash heating at 1500 K several times with direct current passing through the Si wafer. First, one monolayer (ML) of Tl was deposited onto the clean Si(111)-7 $\times$ 7 surface at 500 K to form the Si(111)-1 $\times$ 1-Tl reconstruction. Then, 1/3 ML of Pb was deposited at room temperature to get the Si(111)-$\sqrt{3} \times \sqrt{3}$-(Tl, Pb) 2D surface alloy. During the sample preparation, the RHEED pattern was checked to confirm occurrence of the desired surface reconstructions.

*Present address: Department of Physics, University of Hamburg, D-20355 Hamburg, Germany.

†Present address: International Center for Materials Nanoarchitectonics (MANA), National Institute for Materials Science, 1-1, Namiki, Tsukuba, Ibaraki 305-0044, Japan.

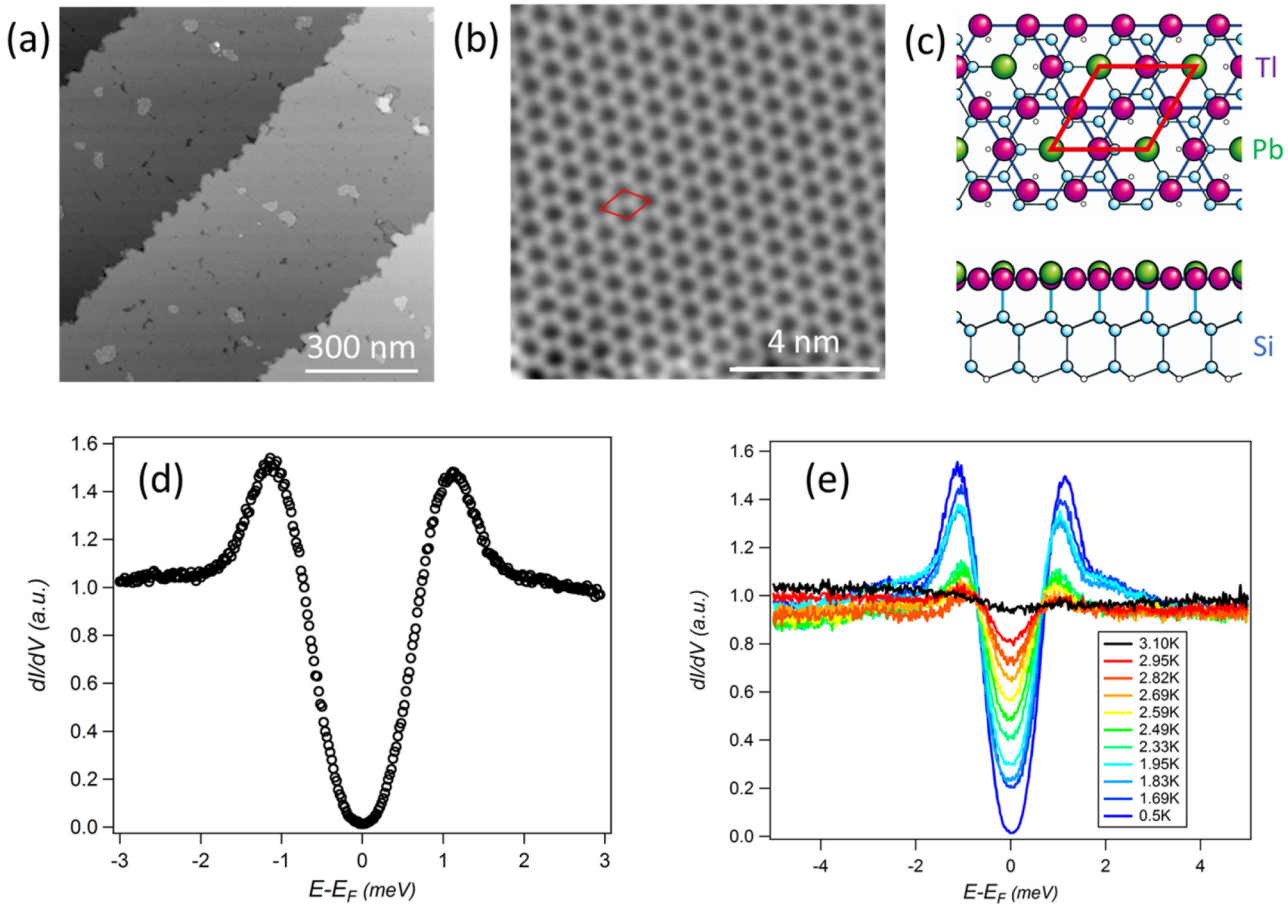

FIG. 1. (a) STM image of Si(111)-$\sqrt{3} \times \sqrt{3}$-(Tl, Pb) at $T < 0.5$ K, with the bias voltage $V_{\text{set}} = 80$ mV and the tunneling current $I_{\text{set}} = 0.015$ nA. (b) Its high-resolution STM image at $T < 0.5$ K, $V_{\text{set}} = 80$ mV, and $I_{\text{set}} = 0.3$ nA. (c) Schematics (upper: plane view; lower: sectional view) of the atomic arrangement. (d) The tunneling spectrum measured at $T < 0.5$ K. The tunneling current was set $I_{\text{set}} = 1$ nA with the tunneling bias voltage $V_{\text{set}} = 1.5$ V, superimposed with the modulation amplitude $V_{\text{ac}} = 0.07$ mV at frequency $f = 971$ Hz for lock-in detection. (e) A series of spectra as a function of temperature. The measurement condition is the same as (d).

Figures 1(a) and 1(b) show STM topography of the Si(111)-$\sqrt{3} \times \sqrt{3}$-(Tl, Pb) surface superstructure measured at $T < 0.5$ K. As shown in Fig. 1(a), the sample has an atomically flat surface and low density of domain boundaries. In the high-resolution STM image [Fig. 1(b)], a honeycomblike structure having a $\sqrt{3} \times \sqrt{3}$ periodicity with respect to the Si(111) substrate is observed. Bright protrusions correspond to the Tl trimers and dark depressions indicate sites occupied by Pb atoms. Pb atoms are known to be located at the centers of the kagome lattice made of Tl atoms [Fig. 1(c)] [17]. We also performed STS measurements and observed the superconducting gap with coherence peaks around $E \pm 1$ meV, as displayed in Fig 1(d). Figure 1(e) shows temperature dependence of the normalized tunneling spectra. The superconducting gap becomes smaller as the temperature increases, and finally it disappears around 3.1 K. Although this critical temperature (T_C) is slightly higher than that determined in the transport measurement (2.25 K) [6], it can be explained by the difference between the local (STS) and global (transport) measurements; the deviation in T_C between STS and transport measurements was reported also for the indium double-atom-layer superconductor [3,5]. The voltage difference between the coherence peaks in Fig. 1(d) is 2.3 meV, from which the size of the superconducting gap can be roughly estimated. The ratio between twice the superconducting energy gap 2Δ and $k_B T_C$, $2\Delta/k_B T_C$ (k_{B} is the Boltzmann constant) is roughly estimated to be 8.6 for the present system (T_C is assumed as 3.1 K). It is much larger than 3.5, the value expected from the Bardeen-Cooper-Schrieffer (BCS) theory. It is also much larger than those of the other atomic-layer superconductors such as Si(111)-$\sqrt{7} \times \sqrt{3}$-In ($2\Delta/k_B T_C = 4.16$), Si(111)-$\sqrt{7} \times \sqrt{3}$-Pb ($2\Delta/k_B T_C = 4.12$), and Si(111)-SIC-Pb ($2\Delta/k_B T_C = 4.4$) [3]. The large BCS ratio suggests an unconventional superconductivity of Si(111)-$\sqrt{3} \times \sqrt{3}$-(Tl, Pb). Moreover, the tunneling spectra at the lowest temperature [Fig. 1(d)] looks like a V shape rather than a U shape. However, there are some differences between our experimental spectra and simple V-shape spectra observed in d-wave superconductors; a linear shape from the bottom to the coherence peak and a rounded shape at the vicinity of the bottom. In general, V-shape spectra result from nodal superconducting gaps, while U-shape spectra are observed in conventional s-wave superconductors [3,18].

Let us discuss the gap shape in more detail. Figure 2 shows an experimental tunneling spectrum (open circles) taken at the lowest temperature (<0.5 K) and theoretically calculated ones

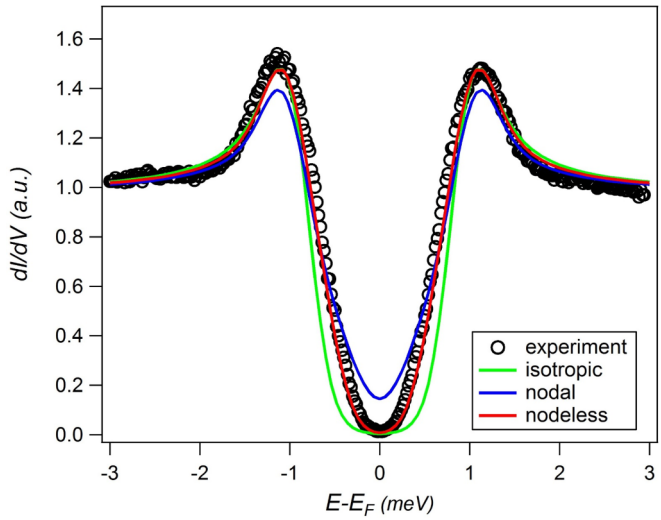

FIG. 2. Tunneling spectrum calculated with the isotropic gap function (green: $\Delta_0 = 0.88$ meV, $\Gamma = 63\,\mu$eV), the nodal gap function (blue: $\Delta_1 = 1.05$ meV, $\Gamma = 1.0\,\mu$eV), and the nodeless gap function (red: $\Delta_0 = 0.48$ meV, $\Delta_1 = 0.92$ meV, $\Gamma = 1.0\,\mu$eV). The extrinsic broadening effect including rf noise and lock-in bias modulation (0.25 meV in total) is considered in these calculations.

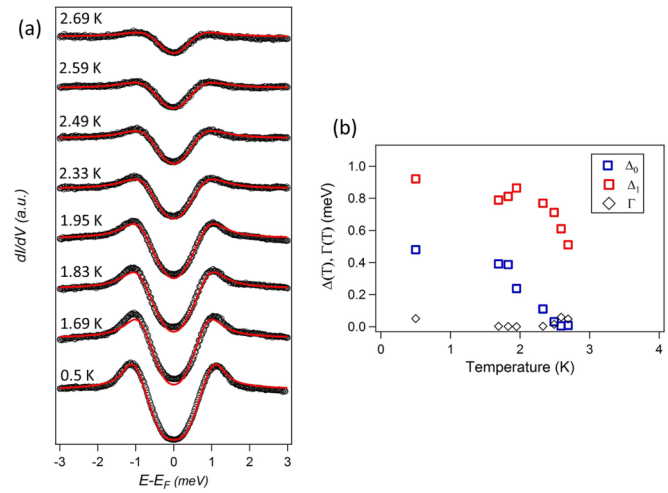

FIG. 3. (a) A series of STS spectra as a function of temperature (open circles) and fitting curves (red curves). Eq. (1) is used for fitting other than the curve of 0.5 K. (b) Temperature dependence of Δ_0, Δ_1, and Γ without magnetic field.

[green, blue, and red curve]. The Dynes formula was used for calculation, as [19]

$$\frac{dI}{dV}(V_S) \propto \int dE \int d\theta\, Re\left\{\frac{|E|\text{-}i\Gamma}{\sqrt{(E\text{-}i\Gamma)^2\text{-}\Delta(\theta)^2}}\right\} \times \frac{\partial f(E+eV_S)}{\partial V}, \quad (1)$$

where f, V_S, and Γ are the Fermi distribution function, bias voltage, and broadening parameter, respectively. Furthermore, the extrinsic broadening effect including rf noise and lock-in bias modulation should be considered at low temperature. It is modeled by Gaussian-type additional convolution to the ideal spectrum [20].

$$\left[\frac{dI}{dV}(V_S)\right]_{\text{conv}} = A\int \exp\left(-\frac{u^2}{2}\right)\cdot\frac{dI}{dV}\left(V_S + u\cdot\frac{B}{\sqrt{2}}\right)du, \quad (2)$$

where V_S, A, and B are the bias voltage, the constant, and the strength of the broadening effect, respectively. The value of B was determined by fitting of the superconducting gap of Pb film, and it is 0.25 meV. The green curve in Fig. 2 indicates the result of numerical fitting with Eqs. (1) and (2) assuming the isotropic gap function [$\Delta(\theta) = \Delta_0$; $\Delta_0 = 0.88$ meV, $\Gamma = 63\,\mu$eV]. It does not reproduce the shape of the spectrum inside the superconducting gap; e.g., the experimental result shows a much sharper gap shape than the isotropic one. However, it is not a prominent V shape like the blue curve, which is fitting by the nodal gap function [$\Delta(\theta) = \Delta_0\cos\theta$; $\Delta_0 = 1.05$ meV, $\Gamma = 1.0\,\mu$eV]. The blue curve also deviates from the experimental data, particularly in the vicinity of the Fermi level. The red curve in Fig. 2 is obtained when we fit the data assuming an anisotropic nodeless gap function [$\Delta(\theta)^2 = {\Delta_0}^2 + {\Delta_1}^2\cos^2\theta$; $\Delta_0 = 0.48$ meV, $\Delta_1 = 0.92$ meV, $\Gamma = 1.0\,\mu$eV]. It reproduces the experimental gap shape better than the others. These fitting results suggest that the superconducting gap of Si(111)-$\sqrt{3}\times\sqrt{3}$-(Tl, Pb) has an anisotropic component.

To gain further insight into the anisotropic gap, we look at the temperature dependence of the spectra. Experimental data and numerical fitting with Eq. (1) are shown in Fig. 3(a) and the temperature variation of Δ_0, Δ_1, and Γ are shown in Fig. 3(b). Δ_0 and Δ_1 decrease as temperature increases but their vanishing temperature looks different. While Δ_0 disappears around 2.6 K, Δ_1 remains. The different temperature dependence of the superconducting gap was observed in a weakly interacting two-band superconductor [21]. This model is consistent with the fact that the Si(111)-$\sqrt{3}\times\sqrt{3}$-(Tl, Pb) has two Fermi surfaces [6].

Let us focus now on the behavior of the superconducting gap under magnetic field. Figures 4(a)–4(d) show mappings of the zero bias conductance (ZBC), superimposed on the STM surface topography, under surface-normal magnetic field. The color code indicates the value of ZBC and the heights in figures indicate the topographic information. The ZBC is low and almost constant over the surface in the absence of the magnetic field [Fig. 4(a)], indicating that the superconducting gap opens uniformly over the whole sample surface. As seen in Figs. 4(b) and 4(c), vortices appear with application of the magnetic field, and the number of vortices increases as the magnetic field increases. Inhomogeneity of the vortex shapes and ZBC mapping observed in Figs. 4(b) and 4(c) seem to be caused by defects such as extra Tl, Pb, and Si adatoms forming clusters or vacancies which can pin vortices. The defects could affect arrangement of vortices and zero bias conductance. The ZBC is uniformly high over the surface at 1.2 T [Fig. 4(d)], which looks like a breakdown of the superconductivity, while, as will be mentioned below, the superconducting gap is not completely closed there.

Figures 5(a) and 5(b) show ZBC mapping around a vortex on a terrace under the magnetic field ($B = 0.2$ T) and a series of tunneling spectra measured across the vortex point by point

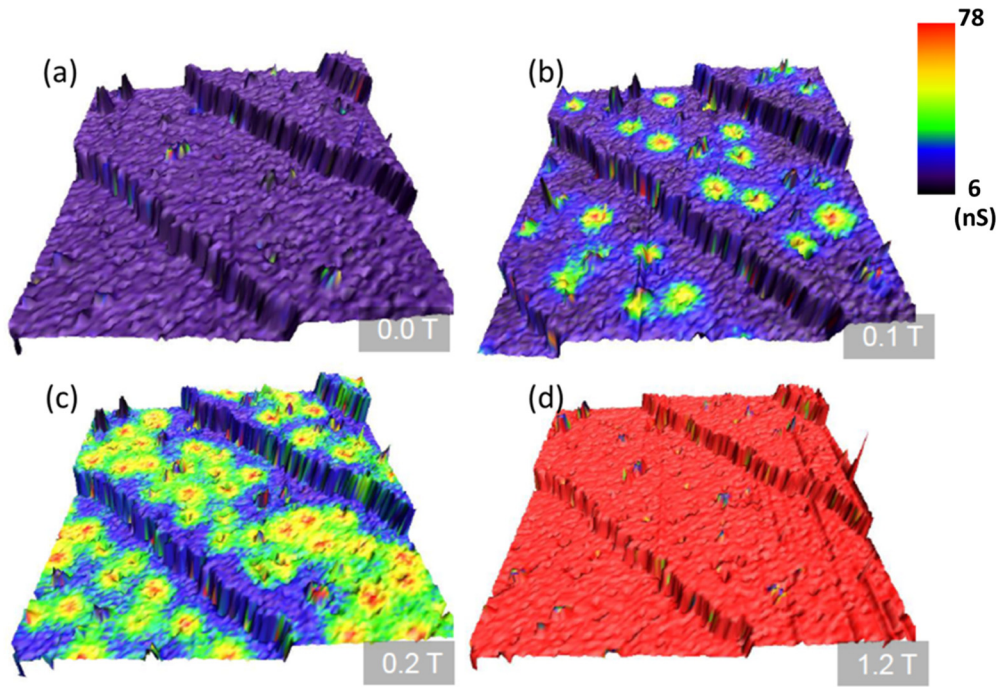

FIG. 4. (a–d) The ZBC mappings (color code), superimposed on the topographic images (height) under surface-normal magnetic field B, measured at $T < 0.5$ K. The scan area is 1 μm × 1 μm. The tunneling current was set $I_{set} = 1$ nA with the tunneling bias voltage $V_{set} = 1.5$ V, superimposed with the modulation amplitude $V_{ac} = 0.07$ mV at frequency $f = 971$ Hz for lock-in detection. The applied magnetic field in (a–(d) is $B = 0$, 0.1, 0.2, and 1.2 T, respectively.

at the positions indicated in Fig. 5(a), respectively. The colors of the spectra correspond to the locations where the spectra were taken. Surprisingly, the dip structure around the Fermi level is not completely closed even at the center of the vortex. Note that this prominent dip structure like a pseudogap does not appear in vortices of other atomic-layer superconductors, e.g., Si(111)-$\sqrt{7} \times \sqrt{3}$-In [22], where the gap completely disappears at the vortex core. Josephson vortices which locate on step edges are also known to have a finite gap remaining at the vortex center. However, Josephson vortices are different from our case because they should have an anisotropic shape. Josephson vortices which locate at weak links such as at step edges and domain boundaries have a finite gap remaining at the vortex center and have elongated shapes. However, since our vortices with the dip structure locate even on terraces without domain boundaries and are isotropic in shape, they are not Josephson vortices.

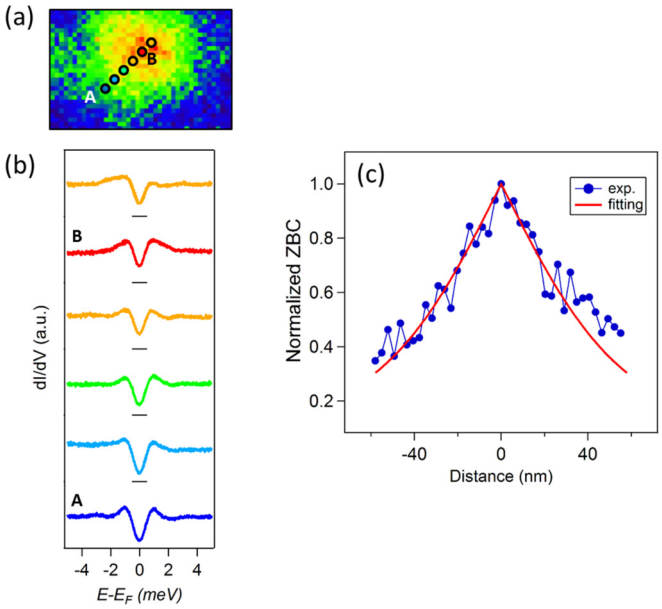

FIG. 5. (a) ZBC mapping around a vortex at $B = 0.2$ T. (b) A series of tunneling spectra measured across the vortex at positions indicated in (a). The color of the spectra indicates the point for measurement in (a). The spectra are offset vertically. (c) ZBC measured across a vortex (blue points) and theoretical fitting using Eq. (3) (red curve). Experimental points are normalized with respect to the value at the vortex center. Zero point on the x axis corresponds to the center of the vortex.

The effective coherence length can be estimated from the size of the vortices. Figure 5(c) shows the ZBC which is normalized so that the value of ZBC at the center of the vortex becomes 1 (blue point) as a function of the distance from the vortex core, and a fitting curve of ZBC (red curve). The following equation derived from the Ginzburg-Landau expression for the superconducting order parameter at $T = 0$ is used for fitting:

$$\sigma(r, 0) = \sigma_0 + (1\text{-}\sigma_0)\left[1\text{-}\tanh\left(\frac{r}{\sqrt{2}\xi}\right)\right]. \qquad (3)$$

σ_0, r, and ξ are the normalized ZBC at a place far away from the vortex, the distance from the vortex center, and the effective coherence length, respectively. We acquired σ_0 and ξ as the fitting parameter to obtain $\sigma_0 = 0.1$ and $\xi = 39.8 \pm 2.2$ nm. We chose the vortex away from the clusters or vacancies for fitting. The effective coherence length is

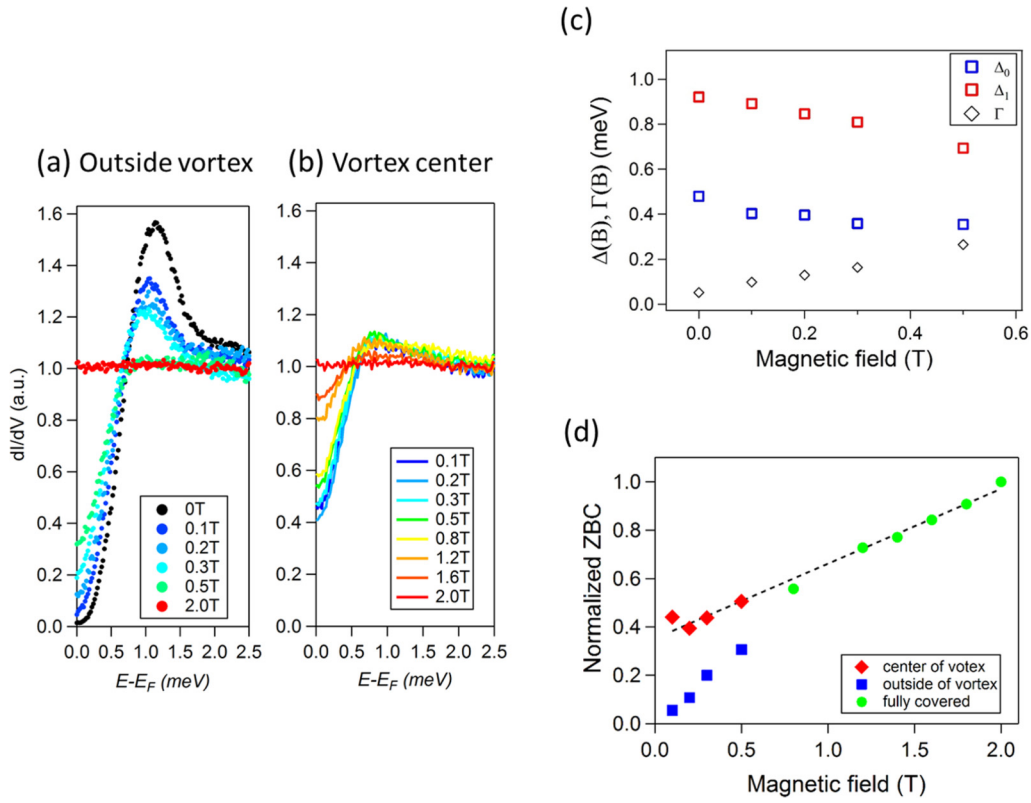

FIG. 6. (a,b) The tunneling spectra measured (a) outside vortices and (b) at the vortex center under different magnetic fields. (c) Magnetic field dependence of Δ_0, Δ_1, and Γ outside the vortex. (d) The magnetic field dependences of ZBC, measured outside vortices (blue), at the vortex center (red), and above 0.8 T (green) where vortices cover the whole surface. The dashed line is a guide to the eye.

comparable to the mean free path which is estimated from resistivity in the normal state and a wave number of the Fermi surface [6]. It is consistent with a picture of dirty superconductors where vortex-bound states are not observed [23].

Let us consider next the field dependence of the superconducting gap and pseudogap. Figures 6(a) and 6(b) show the STS spectra outside (a) and at the vortex center (b) under different magnetic fields. They show that the gap structures vanish with increasing magnetic field in both cases. We tried to fit the superconducting gap under magnetic field with Eq. (1). As a result, Fig. 6(c) shows the magnetic field dependence of Δ_0, Δ_1, and Γ outside the vortex below 0.8 T where the broadening parameter is smaller than the superconducting gaps Δ_0 and Δ_1, both of which become smaller with the magnetic field. The broadening parameter Γ becomes larger than the superconducting gaps Δ_0 and Δ_1 above 0.8 T, both at the center of the vortex and outside of the vortex.

Figure 6(d) shows the field dependence of ZBC outside (blue) and at the vortex center (red). Above 0.8 T, vortices fully cover the whole surface, meaning that a pseudogap remains uniformly over the entire surface as shown in Fig. 4(d). Furthermore, this value of the magnetic field ~0.8 T is close to the macroscopic critical magnetic field determined in the transport measurements (0.67 ± 0.02 T at 0 K) [6]. This suggests that the pseudogap remains in spite of the disappearance of superconductivity above 0.8 T. The pseudogap disappears at ~2.0 T, resulting in almost flat spectra as in Figs. 6(a) and 6(b) (red lines).

Finally, let us discuss the origin of the pseudogap. It cannot be explained by the effect of the superconducting tip where Pb or Tl atoms adhere to the apex of the PtIr tip because the shape of the tunneling spectra does not seem to be a convolution of two superconducting gaps and the signature of Josephson current is not observed in the tunneling spectra with the minimal tip-sample distance (see Supplemental Material [24], S1). If the tip becomes superconducting, the tunnel junction becomes a superconductor-insulator-superconductor junction and Josephson current can be observed when the tunneling resistance is rather small. The absence of the Josephson feature and subgap structures due to multiple Andreev reflection and preserved spectral shape for conventional superconductor-normal junctions (Z~5.0 case in Blonder-Tinkham-Klapwijk theory [25]) is strong evidence that the tip is not in a superconducting state. It should also be noted that, in the Si(111)-$\sqrt{3} \times \sqrt{3}$-(Tl, Pb) system, disorder plays a less important role as compared to the case of a Pb monolayer on Si(111) [16]. As one can see in Fig. 4(a), the former monolayer has no prominent spatial distribution of the superconducting gap while the latter monolayer has strong inhomogeneity, which dramatically affects the gap shape and magnetic responses [16]. One possibility for explaining the pseudogap is a magnetic-field-induced superconductor-insulator-metal transition [26]. An insulator phase corresponding to the pseudogap (having incoherent Cooper pairs) appears inside the vortex and goes into a (normal-state) metallic phase as the applied magnetic field increases (by breaking the Cooper pairs). Another possibility

is a coreless vortex which comes from the spin-triplet component of Cooper pairs. The order parameter of the spin-triplet superconductor has three components because a spin-triplet Cooper pair has the degree of freedom of spin. In such a case, the order parameters do not have to become zero at the vortex center, which is called a coreless vortex [27]. In fact, this system has largely spin-split bands ($\Delta k_{\parallel} = 0.038$-$0.050\,\text{Å}^{-1}$ and $\Delta E = 140$–$250\,\text{meV}$ at E_F) due to strong spin-orbit coupling [6,16], which allows a mixing of spin-singlet and -triplet Cooper pairs [13,28].

To summarize, we have found unconventional superconducting properties of the Si(111)-$\sqrt{3} \times \sqrt{3}$-(Tl, Pb) one-atom-layer alloy, the anisotropy of the superconducting gap, and the pseudogaplike structure in the presence of magnetic field. The pseudogaplike structure suggests the possibility of mixing spin-singlet and -triplet Cooper pairs or a superconductor-insulator-metal transition. Si(111)-$\sqrt{3} \times \sqrt{3}$-(Tl, Pb) is a new example of an unconventional 2D superconductor which can offer an attractive platform to study the relationship among superconductivity, space-inversion symmetry breaking, and large spin-orbit coupling. It could promote further experimental and theoretical investigations.

We acknowledge fruitful discussion with R. Akiyama and R. Hobara, and also financial support from the Japan Society of Promotion of Science (KAKENHI Grants No. 15H02105, No. 16H02108, No. 25246025, and No. 22246006), Japan-Russia Bilateral Program, MEXT (Grant-in-Aid for Scientific Research on Innovative Areas "Molecular Architectonics," Grant No. 25110010), and the Russian Foundation for Basic Research (Grant No. 16-52-50049).

T.N. and H.K. contributed equally to this study.

[1] D. B. Haviland, Y. Liu, and A. M. Goldman, Phys. Rev. Lett. **62**, 2180 (1989).

[2] S. Y. Qin, J. D. Kim, Q. Niu and C. K. Shih, Science **324**, 1314 (2009).

[3] T. Zhang, P. Cheng, W. J. Li, Y. J. Sun, G. Wang, X. G. Zhu, K. He, L. Wang, X. Ma, X. Chen *et al.*, Nat. Phys. **6**, 104 (2010).

[4] T. Uchihashi, P. Mishra, M. Aono, and T. Nakayama, Phys. Rev. Lett. **107**, 207001 (2011).

[5] M. Yamada, T. Hirahara, and S. Hasegawa, Phys. Rev. Lett. **110**, 237001 (2013).

[6] A. V. Matetskiy, S. Ichinokura, L. V. Bondarenko, A. Y. Tupchaya, D. V. Gruznev, A. V. Zotov, A. A. Saranin, R. Hobara, A. Takayama, and S. Hasegawa, Phys. Rev. Lett. **115**, 147003 (2015).

[7] H. Nama, H. Chena, T. Liub, J. Kima, C. Zhanga, J. Yongc, T. R. Lembergerc, P. A. Kratzd, J. R. Kirtleyd, K. Molerd *et al.*, Proc. Natl. Acad. Sci. USA **113**, 10513 (2016).

[8] S. Ichinokura, K. Sugawara, A. Takayama, T. Takahashi, and S. Hasegawa, ACS Nano **10**, 2761 (2016).

[9] T. Sekihara, R. Masutomi, and T. Okamoto, Phys. Rev. Lett. **111**, 057005 (2013).

[10] Y. Saito, Y. Nakamura, M. S. Bahramy, Y. Kohama, J. Ye, Y. Kasahara, Y. Nakagawa, M. Onga, M. Tokunaga, T. Nojima *et al.*, Nat. Phys. **12**, 144 (2016).

[11] H. M. Zhang, Y. Sun, W. Li, J. P. Peng, C. L. Song, Y. Xing, Q. Zhang, J. Guan, Z. Li, Y. Zhao *et al.*, Phys. Rev. Lett. **114**, 107003 (2015).

[12] J. F. Ge, Z. L. Liu, C. Liu, C. L. Gao, D. Qian, Q. K. Xue, Y. Liu, and J. F. Jia, Nat. Mater. **14**, 285 (2015).

[13] L. P. Gor'kov and E. I. Rashba, Phys. Rev. Lett. **87**, 037004 (2001).

[14] E. Bauer, G. Hilscher, H. Michor, Ch. Paul, E. W. Scheidt, A. Gribanov, Yu. Seropegin, H. Noël, M. Sigrist, and P. Rogl, Phys. Rev. Lett. **92**, 027003 (2004).

[15] N. Kimura, K. Ito, K. Saitoh, Y. Umeda, H. Aoki, and T. Terashima, Phys. Rev. Lett. **95**, 247004 (2005).

[16] C. Brun, T. Cren, V. Cherkez, F. Debontridder, S. Pons, D. Fokin, M. C. Tringides, S. Bozhko, L. B. Ioffe, B. L. Altshuler *et al.*, Nat. Phys. **10**, 444 (2014).

[17] D. V. Gruznev, L. V. Bondarenko, A. V. Matetskiy, A. A. Yakovlev, A. Y. Tupchaya, S. V. Eremeev, E. V. Chulkov, J. P. Chou, C. M. Wei, M. Y. Lai *et al.*, Sci. Rep. **4**, 4742 (2014).

[18] C. Manabe, M. Oda, and M. Ido, J. Phys. Soc. Jpn. **66**, 1776 (1997).

[19] R. C. Dynes, V. Narayanamurti, and J. P. Garno, Phys. Rev. Lett. **41**, 1509 (1978).

[20] W. Ulmer and W. Kaissl, Phys. Med. Biol. **48**, 707 (2003).

[21] S. Mukhopadhyay, G. Sheet, P. Raychaudhuri, and H. Takeya, Phys. Rev. B **72**, 014545 (2005).

[22] S. Yoshizawa, H. Kim, T. Kawakami, Y. Nagai, T. Nakayama, X. Hu, Y. Hasegawa, and T. Uchihashi, Phys. Rev. Lett. **113**, 247004 (2014).

[23] Ch. Renner, A. D. Kent, Ph. Niedermann, Ø. Fischer, and F. Lévy, Phys. Rev. Lett. **67**, 1650 (1991).

[24] See Supplemental Material at http://link.aps.org/supplemental/10.1103/PhysRevB.98.134505 for tunneling spectra as a function of conductance. It shows tunneling spectra at different tip-sample distance and no signature of Josephson currents in the contact region.

[25] G. E. Blonder, M. Tinkham, and T. M. Klapwijk, Phys. Rev. B **25**, 4515 (1982).

[26] T. I. Baturina, D. R. Islamov, J. Bentner, C. Strunk, M. R. Baklanov, and A. Satta, JETP Lett. **79**, 337 (2004).

[27] E. Pechenik, B. Rosenstein, B. Ya. Shapiro, and I. Shapiro, Phys. Rev. B **65**, 214532 (2002).

[28] K. C. Weng and C. D. Hu, Sci. Rep. **6**, 29919 (2016).

Supplementary Material for Unconventional Superconductivity at Si(111)-√3×√3-(Tl, Pb) One-Atom-Layer Alloy

T. Nakamura, H. Kim, S. Ichinokura, A. Takayama, A.V. Zotov, A.A. Saranin,
Y. Hasegawa, and S. Hasegawa

S1. Tunneling Spectra as a function of conductance

Even when the contact region (tunnel conductance ~ G_0), there is no any signature of Josephson current such as a Josephson peak in the spectra.

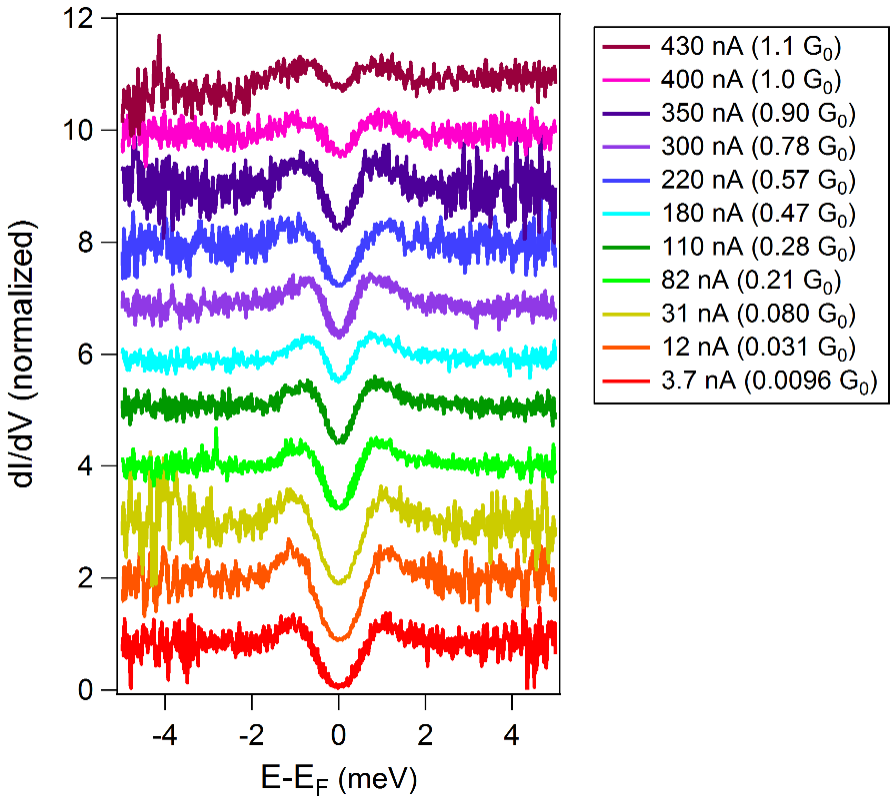

Figure S1.
Series of tunneling spectra measured at different tip-sample distance. The red spectrum is set as the reference, and the legend indicates the tunneling current and the tunneling conductance. G_0 represents quantized conductance.